

# New techniques for laser scattering in plasmas

A. E. Dangor, A. K. L. Dymoke-Bradshaw, and A. Dyson  
Imperial College, London SW7, England

(Received 3 May 1988; accepted for publication 3 August 1988)

We report novel techniques for the scattering of laser light from plasmas to measure density and temperature. Subnanosecond laser pulses are used with fast optical streak cameras to monitor the dispersed scattered light. The spectra are recorded on photographic film. Time resolution down to 100 ps is obtained and stray light problems are eliminated so that the unshifted scattered light can be observed. The techniques have been used to measure densities in the range  $n_e \approx 10^{16}$ – $10^{18}$  cm $^{-3}$  and electron temperatures in the range  $T_e \approx 5$ –35 eV with an accuracy of better than 10%. Laser pulses at 5265 Å with an energy of about 10 J are used and give little plasma heating.

## I. INTRODUCTION

In this paper we review the laser scattering techniques that have been used in recent experiments at the Rutherford Appleton Laboratory to measure the temperature and density of a hydrogen plasma. The aims of these experiments were to determine the heat flux in a laser-heated plasma<sup>1</sup> and the generation of a uniform fully ionized plasma in hydrogen by multiphoton ionization.<sup>2</sup> In another experiment<sup>3</sup> these techniques were employed to investigate the excitation of a large amplitude electrostatic wave formed by the optical mixing of two copropagating laser beams.<sup>4</sup> In the experiments the plasma density was in the range  $10^{16}$ – $10^{18}$  cm $^{-3}$  and the electron temperature in the range 5–35 eV. For this regime, laser scattering is very useful as the plasma self-emission is very much less than the scattered light.<sup>5</sup>

The scattering techniques used are characterized by various novel features. These are subnanosecond laser pulses, fast optical streak cameras to view the dispersed profiles, and photographic film to record the spectra. The use of a short laser pulse gives exceptionally good time resolution, and eliminates both stray light problems and the need for laser and viewing dumps. This is due to the laser pulse length being much smaller than the transit time of the scattering chamber so that time discrimination between stray and scattered light is possible. The unshifted scattered light signal can be monitored so that both the electron and ion features are obtained. The perturbation due to the probe beam is small since, for the same total scattered light, there is less plasma heating for short laser pulses. This is due to the saturation of inverse bremsstrahlung by the strong field effect.<sup>6</sup>

The new scattering techniques described give a continuous spectrum in a single laser shot. The cost per resolved spectral element is much smaller than for photomultiplier-based detection systems. The time dispersion of the streak camera enables simultaneous scattering at complementary angles to be made in one detector channel. By using multiple probe pulses the time evolution of the plasma can also be obtained. A detector dynamic range greater than 1000 has been achieved.

In Sec. II of this paper we describe the experiments performed using the new techniques. The method of obtaining the scattered light profiles from the raw film data is given in Sec. III and the use of the profiles to determine the plasma parameters is presented in Sec. IV.

## II. EXPERIMENTS

The experiments were performed with the Vulcan neodymium glass laser at the Rutherford Appleton Laboratory. Each probe beam was generated by frequency doubling the 1.053  $\mu$ m laser light in a KDP crystal. The scattered light was dispersed in a grating spectrometer and monitored with a Hadland Imacon 675 or 500 streak camera fitted with an S20 photocathode and intensifier. The output was recorded on Ilford HP5 film, the characteristic response of which was obtained with a sensitometer.

### A. The heat flux experiment

In this experiment<sup>1</sup> a small volume of hydrogen plasma was heated by inverse bremsstrahlung absorption of a 1.053  $\mu$ m laser beam and the plasma evolution determined at several distances from the focal spot using Thomson scattering of a 5265-Å probe.

A schematic of the arrangement is shown in Fig. 1. A slow Z pinch in hydrogen was used to produce fully ionized plasma. The heating beam, with pulse length 1.5 ns, was focused transversely into the pinch to a spot of 200  $\mu$ m diam-

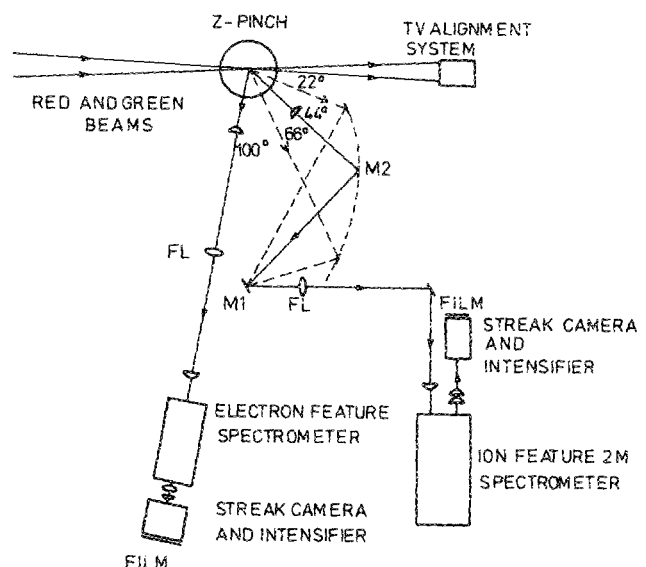


FIG. 1. Schematic of the heat flux experiment. The scattering angle in the ion feature channel was selected by moving the plane mirror  $M_2$  along the ellipse with foci at the plasma and mirror  $M_1$ . FL are field lenses.

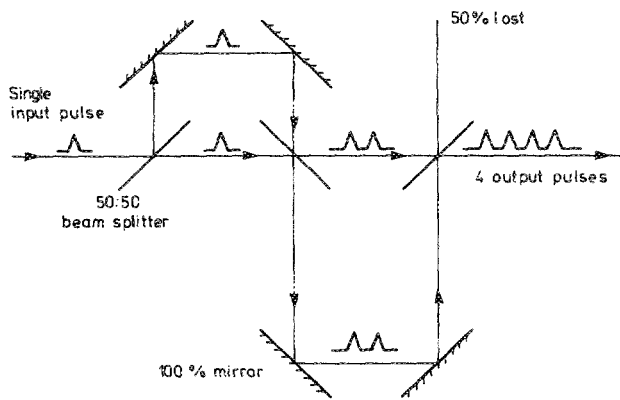


FIG. 2. The pulse-stacker arrangement for producing the four probe pulses.

eter, giving a peak irradiance of  $5 \times 10^{13} \text{ W cm}^{-2}$ . Four probe pulses of 100 ps separated by 1 ns were produced using the pulse-stacker arrangement shown in Fig. 2. These pulses were amplified and frequency doubled to give a total energy of about 20 J. The scattered light from each pulse was monitored in two channels, one at a large angle of  $100^\circ$  and the other at a variable angle of  $22^\circ$ ,  $44^\circ$ , or  $66^\circ$ . The channel collecting light at the large angle had a resolution of  $5 \text{ \AA}$  sufficient to resolve the electron feature but not the central ion feature. The ion feature was resolved in the second channel which had a resolution of  $0.1 \text{ \AA}$ . The electron feature was used to determine the electron density and temperature. The resolved ion feature enabled the ion temperature to be determined and was also used to detect the presence of ion acoustic turbulence. The ion feature was monitored at more than one angle to investigate the ion acoustic energy spectrum. For both channels the collecting optics ( $f/6$ ) consisted of two identical lenses with a field lens at the intermediate focus. The scattering volume was a cylinder of  $100 \mu\text{m}$  diameter and about 1 mm long, coaxial with the probe beam. The temporal resolution was determined by the probe pulse duration of 100 ps. The spatial variation of the plasma temperature and density was obtained by moving the focal spot of the heating beam vertically or horizontally with respect to the fixed scattering volume. For horizontal displacements the differential scattering vector is in the plane of the heat flux while for vertical displacements it is perpendicular to the heat flux. This allowed the effect of the heat flux on the velocity distribution to be investigated.

An example of the data obtained from a typical shot is shown in Fig. 3. The well-defined wings in the electron feature from the first probe pulse, which is before the heating beam, are no longer present in subsequent pulses. This shows that the plasma was heated. There is no change in density on this short timescale. In the absence of a plasma no scattered signal was observed, indicating that there was no stray light. The heating is also evident in the ion feature spectra. The spectra obtained from the first pulse were from a thermal plasma. These were used to obtain a relative sensitivity of the electron and ion feature channels.

The electron and ion temperatures obtained from the scattered spectra at different positions were compared with a 1-d hydrodynamic simulation. This shows<sup>1</sup> that the inverse bremsstrahlung absorption should include the strong field correction and that the maximum heat flux is limited to about 0.1 of the free streaming limit. The ion-electron equilibration rate is found to be in agreement with the usual expression. The ratio of  $T_e/T_i$  was measured as 5. However, the ratio of the total scattered light in the ion and electron features is close to the theoretical value for a thermal plasma, indicating that the level of turbulence excited by the heat flow is small.

### B. The multiphoton ionization experiment

In this experiment<sup>2</sup> an intense 5265-A beam was focused into hydrogen gas at a pressure of a few Torr to investigate the generation of a plasma by multiphoton ionization. Scattered light was monitored from this ionizing laser beam. The laser energy was typically 10 J in 100 ps with a focal spot of about  $200 \mu\text{m}$  radius, giving a peak irradiance of about  $10^{14} \text{ W cm}^{-2}$ .

The experimental arrangement is shown in Fig. 4. Two scattering channels were used at angles of  $120^\circ$  and  $160^\circ$  with respect to the incident beam. Light scattered from the complementary angles,  $60^\circ$  and  $20^\circ$ , respectively, was collected by using spherical mirrors to reimage light back to the scattering volume. In this way spectra with four different values of the scattering parameter  $\alpha$  were obtained. The  $f/4$  collecting optics consisted of two identical lenses with an overall magnification of unity. A pinhole in the image plane of the first lens defined the extent of the scattering volume which was chosen to be of dimension  $100 \mu\text{m}$ . The spectral and temporal resolutions in both channels were about  $5 \text{ \AA}$  and

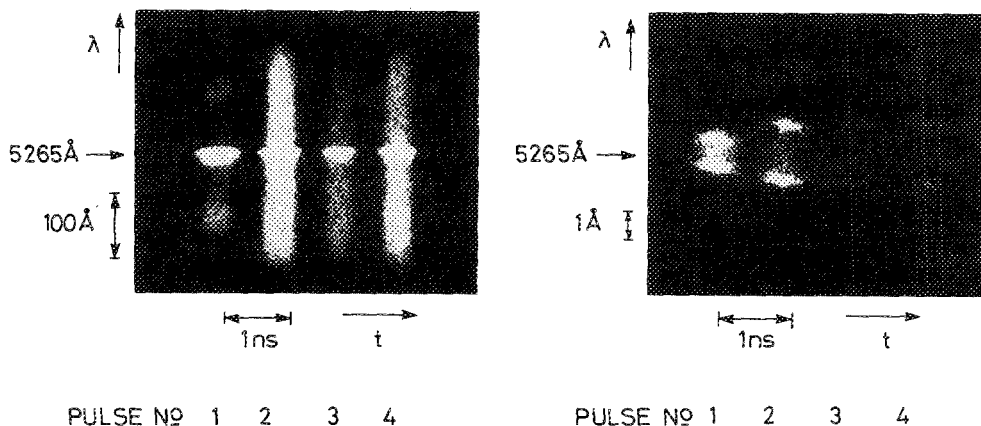


FIG. 3. Typical scattering data from the heat flux experiment using the pulse stacker. The electron features are on the left and the ion features on the right.

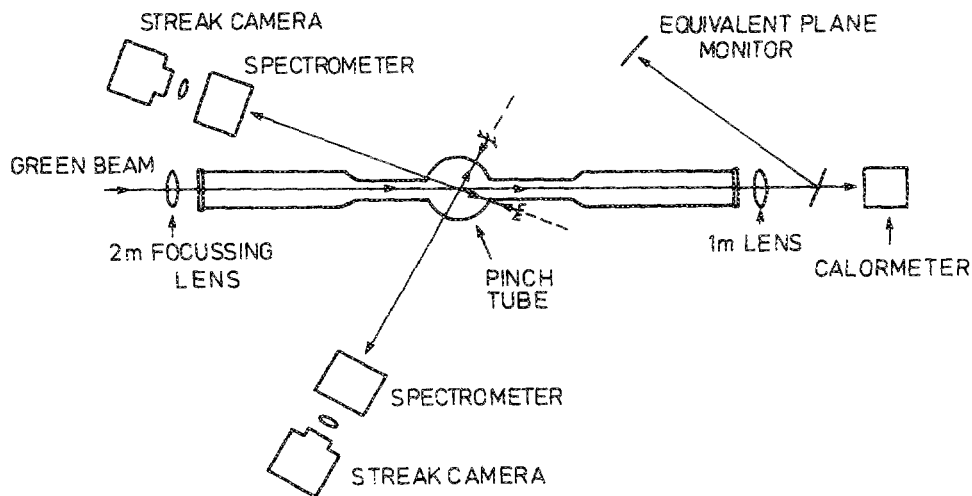


FIG. 4. Schematic of the multiphoton ionization experiment. The scattered light is collected at the complementary angles  $20^\circ, 160^\circ$  and  $60^\circ, 120^\circ$ .

100 ps, respectively. The length of plasma generated was determined by monitoring the scattering at different positions along the axis of the laser beam. The radial extent was determined by viewing the total scattered light in zero order. The laser spot size was measured with the equivalent plane monitor.

An example of the data is given in Fig. 5. This shows two spectra with  $\alpha = 0.9$  and  $\alpha = 5.4$  obtained at  $160^\circ$  and  $20^\circ$ , respectively. The results show that the plasma generated is fully ionized and that it is uniform over an axial length of at least 8 mm. The radial extent is about equal to the laser spot size. The temperature of the plasma is about 10 eV.

### C. The beat wave experiment

The aim of this experiment<sup>3</sup> was to detect the plasma wave generated by mixing two laser beams with wavelengths 1.053 and 1.064  $\mu\text{m}$ . At the irradiances available ( $\approx 2 \times 10^{14} \text{ W cm}^{-2}$ ) the plasma frequency had to be matched to the frequency difference of the pump beams to within 1%.<sup>7</sup> For this reason, multiphoton ionization was used to generate the plasma. The induced plasma wave interacts with the pump beams to produce sidebands at frequencies shifted by the plasma frequency.<sup>8</sup> This can be used to measure the amplitude of the plasma wave generated by the beat wave process. The decay of the plasma wave will also give rise to additional

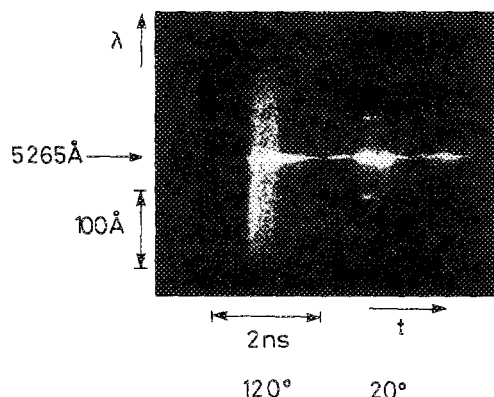


FIG. 5. Scattering data from the multiphoton ionization experiment in hydrogen at 4.0 Torr. The intermediate light at the laser probe wavelength is due to reflections in the target chamber.

heating above that expected from inverse bremsstrahlung absorption of the pump beams.

The experimental arrangement is shown in Fig. 6. The pump beams, each delivering 50 J in 200 ps, were focused ( $f/20$ ) to give a 200- $\mu\text{m}$  radius spot. The plasma was preformed by a 5265- $\text{\AA}$  laser beam of 10 J and 200 ps, copropagating with the pump beams and focused to the same position. The pump beams were mixed in vacuum to avoid Raman scattering by atmospheric nitrogen.<sup>9</sup> The transmitted light was dispersed and then monitored with an Imacon 675 streak camera fitted with an S1 photocathode. Thomson scattered light from the ionizing green beam and from a separate delayed green probe was monitored in two channels. Using this arrangement the plasma conditions could be determined both before and after the pump beams had passed through the plasma.

Figure 7 shows upshifted and downshifted sidebands on the pumps. These are generated by the CARS effect<sup>10</sup> in the optical components in the mixing box and are about an order of magnitude greater than the sidebands expected from the plasma wave. An analysis of this data is to be published elsewhere. Figure 8 shows Thomson scattered spectra with the characteristic features associated with both high and low  $\alpha$ . The temperature increases from 12 eV to about 25 eV. In some shots the spectra obtained with the probe beam, which is after the pump beams, indicate a nonthermal plasma. This could be due to the heating process or due to a two-component plasma consisting of plasma heated by the pump beams and the surrounding plasma generated by the probe beam. The temperature increase is consistent with inverse bremsstrahlung absorption of the pump beams and suggests that there is no additional heating due to the decay of a plasma wave. The density was measured to be  $1.1 \times 10^{17} \text{ cm}^{-3}$  with an accuracy of 10%. The calculated resonant density for the pump beams is  $1.07 \times 10^{17} \text{ cm}^{-3}$  and as indicated previously a large amplitude plasma wave is expected only if the density is within 0.5%. The absence of any additional heating in the experiment may be due to the density being outside this range.

### III. DATA REDUCTION

In this section we describe how the information recorded on the film is converted into spectral profiles that can be

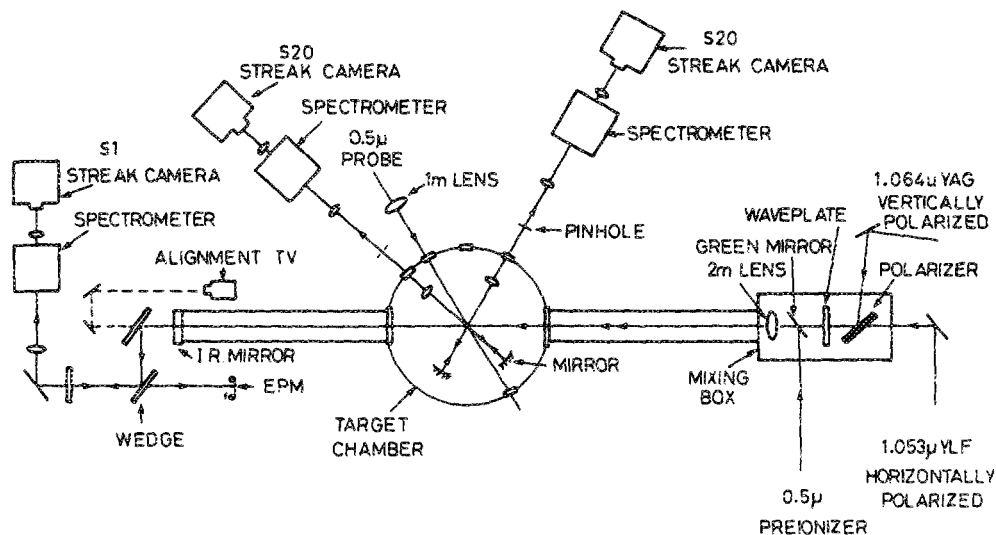


FIG. 6. Schematic of the beat wave experiment. The 1.053- $\mu\text{m}$  and 1.064- $\mu\text{m}$  pump beams are made copropagating and with the same polarization under vacuum in the mixing box. Scattering from the preionizing beam is collected at 40°, 140° in one channel and 58°, 122° in the second channel. The corresponding angles for the probe beam are 18°, 162° and 64°, 116°.

compared to scattering theory. The recorded information is digitized and then corrected for film response, distortion in the image intensifier, and the spectral response of the channel. The spectral resolution of the channel is allowed for when comparing with theoretical spectra.

A Joyce Loebel microdensitometer was used to digitize the film data. The microdensitometer slit width was chosen to match the granular structure on the exposed film. This structure is produced in the intensifier. The slit height was set to match the temporal resolution that is the equal to the duration of the probe pulse. This ensured that the spectral information was not degraded while keeping the fluctuations in the digitized data to a minimum.

The film response was obtained by exposing the film with a sensitometer. This consists of a photographic flash lamp, filtered to give the same output as the camera intensifier phosphor and of duration similar to the phosphor persistence. The light is passed through a ten-level attenuator with 0.3ND steps and then onto the film to give a calibration step wedge. For each shot a calibration wedge was recorded and then processed with the data. The films were scanned with the microdensitometer and the calibration wedge used to convert the density value of each point in the scattered spectrum to the intensity value. A typical wedge and the resulting characteristic curve obtained by linear interpolation are shown in Fig. 9.

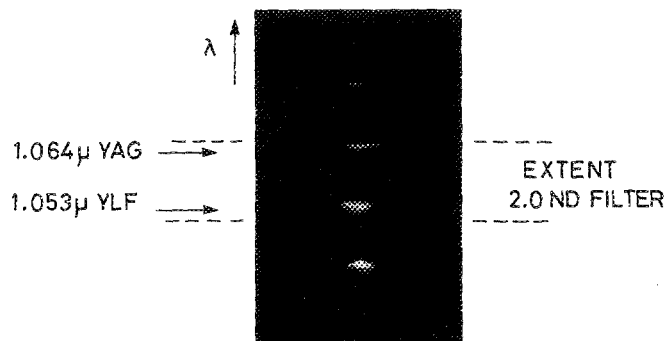


FIG. 7. Upshifted and downshifted sidebands on the pump beams. Light at 1.053 and 1.064  $\mu\text{m}$  is attenuated by 100.

The intensifier used with the Imacon 675 camera uses a Mullard XX1330 (50/40) tube that produces pincushion distortion of the form

$$ar^3 + br = r', \quad (1)$$

where  $r$  and  $r'$  are the distances from the center of distortion in the input and output planes, respectively. The coefficients are  $a = 2.128 \times 10^{-4} \text{ mm}^{-2}$  and  $b = 0.667$ . The intensities in the input and output planes of the intensifier with gain  $G$  are related by

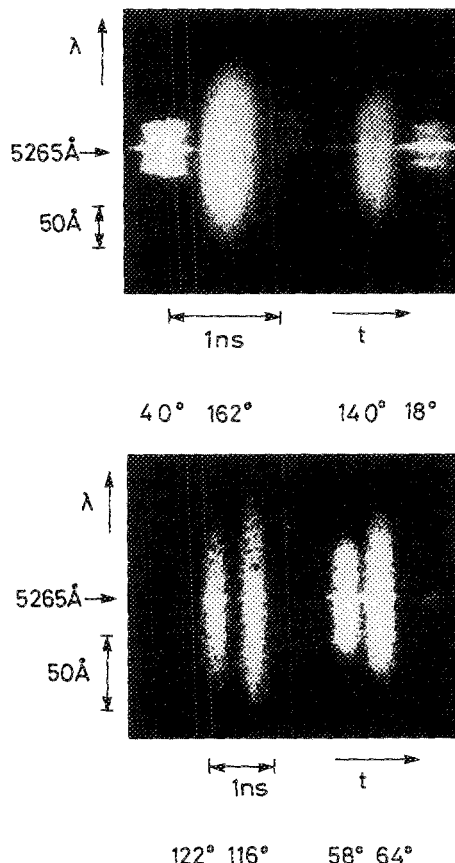


FIG. 8. Thomson scattering data from the beat wave experiment. In both photographs the first and third spectra are from the preionizing beam and the second and fourth spectra are from the probe beam.

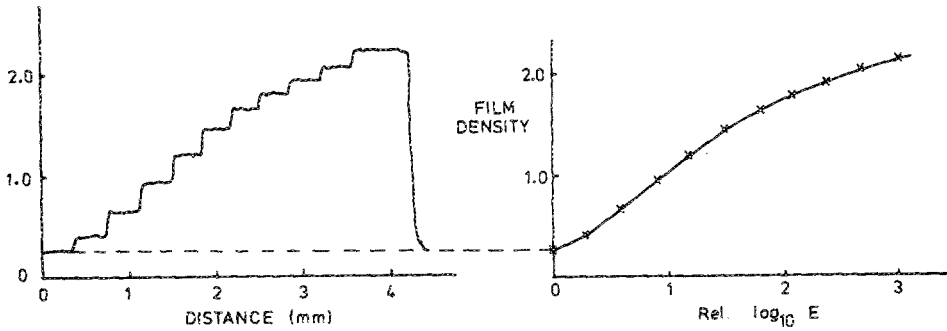


FIG. 9. Characteristic curve for HP5 film (right) obtained from the calibration wedge data (left).

$$GI(r)r dr d\theta = I'(r')r' dr' d\theta$$

so that

$$GI(r) = I'(r')(ar^2 + b)(3ar^2 + b). \quad (2)$$

These equations are used to correct for the distortion. The correction is insignificant for  $r < 5$  mm. The 20/30 intensifier used with the Imacon 500 camera has a correcting lens element and gives low distortion over its whole output field.

The spectral response of each channel was determined by imaging a standard lamp onto the input slit of the spectrometer. Exposures were taken in focus mode and corrected for film response and distortion. The color temperature of the lamp was then used to give the spectral response. Vignetting in the coupling optics between the grating and streak camera as well as the photocathode spectral response are accounted for by this method. Over the spectral region of interest the relative sensitivity changes by about 10%.

The photographic data of weak scattered signals that are obtained with the intensifier at maximum gain are grainy. This is a characteristic of the intensifier and results in large intensity fluctuations in the spectral profiles. In such cases a smoothing routine based on taking the median of a set of surrounding data points is used before fitting to the theoretical profiles.

#### IV. COMPARISON WITH THEORY

A least-squares method is used to fit the reduced data to theoretical Thomson scattering profiles from a thermal plasma which have been corrected for instrument response. The scattered light spectrum lies in one of three domains<sup>5</sup> depending on the value of the scattering parameter  $\alpha$ . This is defined as

$$\alpha = 1/k\lambda_D, \quad (3)$$

where  $\lambda_D$  is the Debye length and  $k$  is the differential scattering vector

$$k = 2k_0 \sin(\theta/2). \quad (4)$$

Here  $k_0 = 2\pi/\lambda$  is the wave vector of the incident light and  $\theta$  is the scattering angle.

For  $\alpha < 0.5$  the light is incoherently scattered from individual electrons and the resulting spectrum is directly related to the electron velocity distribution. For a thermal plasma the shape of the spectrum is predominantly sensitive to electron temperature and is almost Gaussian with the half width at  $1/e$  given by

$$\Delta\omega = kv_e, \quad (5)$$

where  $v_e = (2k_B T_e/m_e)^{1/2}$ , so that for  $\lambda = 5265 \text{ \AA}$ ,

$$T_e = 2.29 \times 10^{-3} [\Delta\lambda(\text{\AA})/\sin(\theta/2)]^2 \text{ eV}. \quad (6)$$

Thus by measuring the width of the profile the electron temperature can be obtained directly. An accurate determination of the electron density can only be obtained if the scattering channel is absolutely calibrated. An example of the fit obtained for a spectrum with  $T_e = 26 \text{ eV}$  and  $\alpha = 0.4$  is shown in Fig. 10. The accuracy on the temperature is better than 10% and  $\alpha$  is better than 25%. The quoted density is obtained from  $T_e$  and  $\alpha$  using Eq. (3). The  $1/e$  point of the profile in the figure is  $110 \text{ \AA}$  and this gives  $T_e = 28 \text{ eV}$  using Eq. (6).

For values of  $\alpha$  between 0.5 and 2 the spectrum consists of a narrow ion feature centered on a broad electron feature. The electron feature has distinct shoulders at approximately

$$\Delta\omega = \alpha kv_e, \quad (7)$$

so that for  $\lambda = 5265 \text{ \AA}$ ,

$$n_e = 7.16 \times 10^{13} [\Delta\lambda(\text{\AA})]^2 \text{ cm}^{-3}. \quad (8)$$

The position is independent of the scattering angle. The detailed shape of the electron feature depends upon both the temperature and density. By fitting theoretical profiles to the observed spectrum the electron density and temperature are determined. The fit obtained to a spectrum with  $T_e = 34 \text{ eV}$  and  $n_e = 6.5 \times 10^{17} \text{ cm}^{-3}$  corresponding to  $\alpha = 1.0$  is shown in Fig. 11. The accuracy on  $T_e$  and  $n_e$  is better than 10%. The shoulders are at  $95 \text{ \AA}$  and this gives  $n_e = 6.5 \times 10^{17} \text{ cm}^{-3}$  confirming that for this range of  $\alpha$  Eq. (8) is accurate enough.

For  $\alpha > 2$  the spectrum has distinct satellites located at

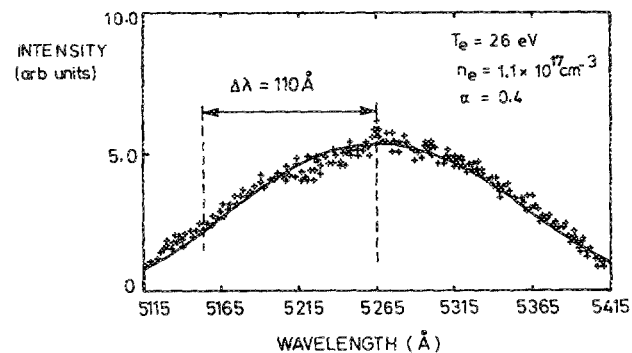


FIG. 10. The scattered profile at  $\theta = 162^\circ$  and the best-fit theoretical curve.

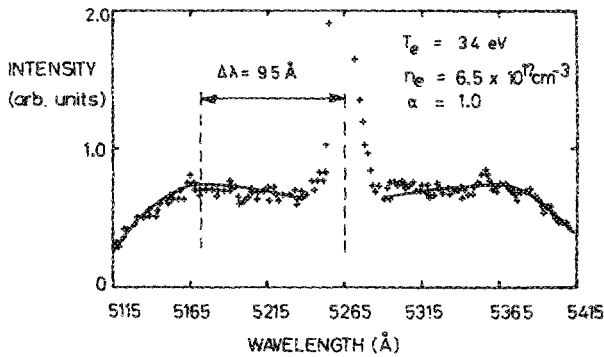


FIG. 11. The scattered profile at  $\theta = 100^\circ$  and the best-fit theoretical electron feature.

$$(\Delta\omega)^2 = \omega_p^2 + 3k^2v_e^2$$

$$= \omega_p^2(1 + 3/\alpha^2), \quad (9)$$

where  $\omega_p$  is the plasma frequency, so that for  $\lambda = 5265 \text{ \AA}$ ,

$$[\Delta\lambda(\text{\AA})]^2 = 6.9 \times 10^{-15} n_e (\text{cm}^{-3})$$

$$+ 650 \sin^2(\theta/2) T_e (\text{eV}). \quad (10)$$

If  $\alpha$  is very large the second term which is temperature dependent is relatively small so that a direct measurement of the density is possible from the satellite positions. Figure 12 shows data obtained in the multiphoton ionization experiment with  $n_e = 2.7 \times 10^{17} \text{ cm}^{-3}$  to an accuracy better than 10%. This value of  $n_e$  has been obtained from Eq. (10) using the fitted temperature from a low  $\alpha$  spectrum. Neglecting the temperature correction gives  $n_e = 2.9 \times 10^{17} \text{ cm}^{-3}$ . The scattered spectra from three axial locations show that the positions of the satellites are the same to better than 2% indicating that the plasma is uniform to better than 4% over at least 8 mm.

For large  $\alpha$  the ion feature contains the greater part of the scattered light. If  $T_e/T_i > 3$  the ion feature has distinct wings that are due to the ion acoustic resonance. The positions are

$$\Delta\omega = k \left( \frac{\alpha^2}{1 + \alpha^2} \frac{k_B T_e}{m_i} + \frac{3k_B T_i}{m_i} \right)^{1/2} \quad (11)$$

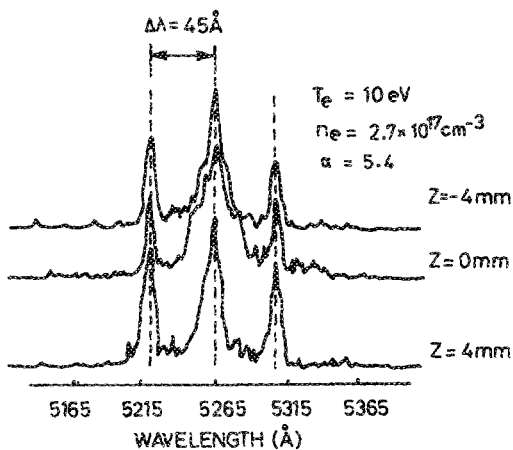


FIG. 12. High  $\alpha$  scattering data from the multiphoton ionization experiment at the focus ( $z = 0$ ) and on either side. The value of  $n_e$  is obtained using the positions of the shoulders with  $T_e$  obtained from a low  $\alpha$  profile.

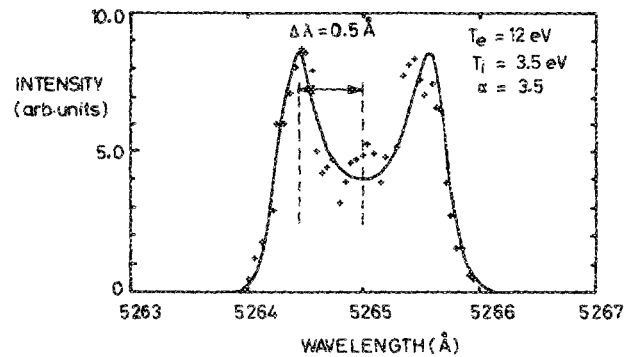


FIG. 13. Ion feature spectrum with the best-fit theoretical curve.

and can be used to determine the ion temperature if the electron density and temperature are known. An example of the fit obtained to the ion feature is shown in Fig. 13. With  $T_e$  known to better than 10% the value of  $T_i$  is accurate to within 20%. Figure 14 shows a spectrum that due to turbulence cannot be fitted to a thermal profile. However, using the position of the wings the ion temperature can still be obtained from Eq. (11). The level of ion acoustic turbulence can be found by comparing the relative magnitudes of the integrated ion and electron features. For the case shown the integrated ion feature is about 1.5 times greater than the thermal value and indicates a level of turbulence  $\delta n/n = 0.09\%$ . This shows the extreme sensitivity of the shape of the ion feature spectrum to turbulence.

## V. DISCUSSION

In the scattering measurements reported in this paper an absolute calibration of the scattering channels was not necessary. This is because scattering was observed at intermediate values of  $\alpha$  or at complementary angles to give extreme values of  $\alpha$ . In the first case both  $T_e$  and  $n_e$  are determined from the shape of the electron feature. In the second case the width of the low  $\alpha$  spectrum gives  $T_e$  and using this value the positions of the satellites in the high  $\alpha$  spectrum give  $n_e$ . The use of short probe pulses with streak camera monitoring is particularly suitable for this. Only one detection channel is necessary when scattering at complementary angles and, if these angles are judiciously chosen, curve fitting is not required. It should be noted that calibration by Ray-

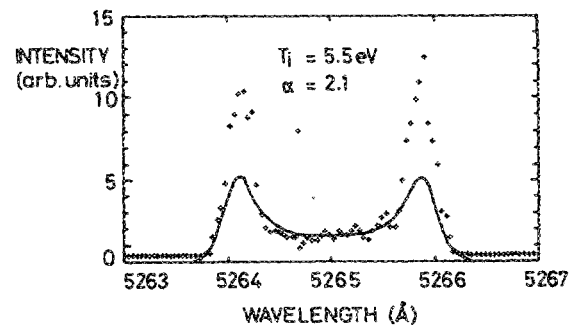


FIG. 14. Ion feature spectrum from the heat flux experiment. The theoretical profile is obtained using  $n_e$  and  $T_e$  from the electron feature in a separate channel and  $T_i$  from the positions of the wings in the ion feature.

leigh scattering is not possible with short probe pulses because of multiphoton ionization.

To obtain  $T_e$  from the ion feature requires that  $T_e$  and  $n_e$  be known and thus it is necessary to observe scattering in more than one channel. This is because the width of the ion feature is considerably less than that of the electron feature, typically about 1/100.

The principal errors in the measured quantities arise from the fitting and the uncertainty in the film response, the spectrometer dispersion, and spectral response. The detection system used gives a continuous spectrum and thus allows the fitting to be done to high accuracy. In these experiments the quoted errors are mainly due to small departures from thermal plasma. An accuracy of better than 10% can be obtained for  $n_e > 5 \times 10^{16} \text{ cm}^{-3}$  for submillimeter size scattering volumes. For lower values of  $n_e$  it is necessary to increase the scattering volume. With  $f/6$  collecting optics and an incident intensity of  $5 \times 10^{13} \text{ W cm}^{-2}$ , the total number of scattered photons into the detector is  $\approx 10^6$  from a scattering volume of  $100 \mu\text{m}$  size and plasma with  $n_e \approx 10^{17} \text{ cm}^{-3}$  and  $\alpha \approx 1$ . Assuming 100 resolved spectral elements and 10% spectrometer throughput this gives  $\approx 10^3$  photons per element on the streak camera photocathode. For the Hadland Imacon 675 camera with intensifier at maximum gain this corresponds to a signal-to-noise level of about 20:1.

## ACKNOWLEDGEMENTS

We would like to thank Margret Lewis, Terence Garvey, Adrian Cole, Christopher Edwards, and Colin Danson for their considerable assistance with the experiments. Our thanks are also due to Ian Ross for suggesting the pulse-stacker arrangement and Roger Evans for helpful discussions.

- <sup>1</sup>A. Dyson, A. E. Dangor, A. K. L. Dymoke-Bradshaw, and R. G. Evans, *Plasma Phys. Contr. Fusion* (to be published).
- <sup>2</sup>A. E. Dangor, A. K. L. Dymoke-Bradshaw, A. Dyson, T. Garvey, I. Mitchell, A. J. Cole, C. N. Danson, C. B. Edwards, and R. G. Evans, *IBEE Trans. Plasma Sci.* **PS-2**, 161 (1987).
- <sup>3</sup>Rutherford Appleton Laboratory Annual Report 1988 (to be published).
- <sup>4</sup>T. Tajima and J. M. Dawson, *Phys. Rev. Lett.* **43**, 267 (1979).
- <sup>5</sup>D. E. Evans and J. Katzenstein, *Rep. Prog. Phys.* **32**, 207 (1969).
- <sup>6</sup>G. J. Pert, *J. Phys. A* **5**, 506 (1972).
- <sup>7</sup>S. J. Karttunen and R. R. E. Salomaa, Helsinki University Report No. TKK-F-A616 (1987).
- <sup>8</sup>S. J. Karttunen and R. R. E. Salomaa, *Phys. Rev. Lett.* **56**, 604 (1986).
- <sup>9</sup>Rutherford Appleton Laboratory Annual Report No. RAL-86-046, p.A1.1 (1986).
- <sup>10</sup>M. Maier, *Appl. Phys.* **11**, 231 (1976).